The PCY-SAG14 phytocyanin module regulated by PIFs and miR408 promotes dark-induced leaf senescence in *Arabidopsis*

Chen Hao[a], Yanzhi Yang[b], Jianmei Du[c], Xing Wang Deng[b,c,1] (ID), and Lei Li[a,b,c,1] (ID)

[a]State Key Laboratory of Protein and Plant Gene Research, School of Life Sciences, Peking University, Beijing 100871, China; [b]School of Advanced Agricultural Sciences, Peking University, Beijing 100871, China; and [c]Peking–Tsinghua Center for Life Sciences, Academy for Advanced Interdisciplinary Studies, Peking University, Beijing 100871, China

Leaf senescence is a critical process in plants and has a direct impact on many important agronomic traits. Despite decades of research on senescence-altered mutants via forward genetics and functional assessment of senescence-associated genes (SAGs) via reverse genetics, the senescence signal and the molecular mechanism that perceives and transduces the signal remain elusive. Here, using dark-induced senescence (DIS) of *Arabidopsis* leaf as the experimental system, we show that exogenous copper induces the senescence syndrome and transcriptomic changes in light-grown plants parallel to those in DIS. By profiling the transcriptomes and tracking the subcellular copper distribution, we found that reciprocal regulation of plastocyanin, the thylakoid lumen mobile electron carrier in the Z scheme of photosynthetic electron transport, and SAG14 and plantacyanin (PCY), a pair of interacting small blue copper proteins located on the endomembrane, is a common thread in different leaf senescence scenarios, including DIS. Genetic and molecular experiments confirmed that the PCY-SAG14 module is necessary and sufficient for promoting DIS. We also found that the PCY-SAG14 module is repressed by a conserved microRNA, miR408, which in turn is repressed by phytochrome interacting factor 3/4/5 (PIF3/4/5), the key trio of transcription factors promoting DIS. Together, these findings indicate that intracellular copper redistribution mediated by PCY-SAG14 has a regulatory role in DIS. Further deciphering the copper homeostasis mechanism and its interaction with other senescence-regulating pathways should provide insights into our understanding of the fundamental question of how plants age.

copper | plastocyanin | blue copper protein | leaf senescence | dark-induced senescence

Postmitotic senescence is the terminal development stage of leaves, the photosynthetic organs of plants. Leaf senescence is characterized by the functional transition from nutrient assimilation to nutrient remobilization, which involves chlorophyll degradation, chloroplast degeneration, and catabolism of macromolecules, eventually leading to cell and organ death (1–3). The released nutrients are exported to other developing organs, such as new leaves or seeds, to ensure fitness or reproductive success (1). Extensive studies on senescence-altered mutants via forward genetics and functional assessment of senescence-associated genes (SAGs) via reverse genetics in the model plant *Arabidopsis* and crop plants have elucidated the roles of phytohormones and identified many genes necessary for manifesting the senescence syndrome (1, 3–6). Despite this knowledge, the senescence signal and the molecular mechanism that perceives and transduces the signal remain elusive.

In addition to age, which is a primary determinant of leaf senescence, an array of unfavorable changes in the ambient surroundings of the plants, such as seasonal day length shift, water limitations, prolonged darkness, extreme temperatures, and nutrition deficiency, can trigger the onset and/or accelerate the progression of leaf senescence (1–3, 7). Because plants use various mechanisms to sense these primary cues (e.g., light and temperature) (8, 9), it is possible that the senescence signal, or a component of it, is a second messenger commonly elicited by these distinct primary signaling systems to activate the senescence program. Though signaling molecules, including phytohormones (1, 4, 6), sugar (1, 10–12), and reactive oxygen species (13), have been shown to play significant roles in both age-dependent and environment-induced leaf senescence, their candidacy as the senescence signal remains debatable.

Indispensable to the Z scheme of photosynthetic electron transport is a mobile electron carrier in the thylakoid lumen that acts between the cytochrome b_6f complex and photosystem I, which in land plants is fulfilled by the conserved small blue copper protein plastocyanin (14–16). Different from other transition metals, redox active copper is highly toxic in its free form. Eukaryotes have evolved a strong chelating capacity in the cytosol that allows for less than one free copper ion per cell (17, 18). Consequently, elaborate transport systems and partition mechanisms are present in eukaryotic cells for the precise allocation of copper to specific target proteins (19, 20). Based on these features of the transition metal, it is tempting to hypothesize that changes in intracellular copper homeostasis, after suppression of photosynthetic electron transport, has a

Significance

Leaf senescence is a critical process in plants and has a direct impact on many important agronomic traits. Despite decades of research, identity of the senescence signal and the molecular mechanism that perceives and transduces the signal remain elusive. Using dark-induced leaf senescence as the experimental system, we found that senescence induces rapid reciprocal regulation of plastocyanin, a copper-binding electron carrier in the photosynthetic electron transport chain, and the PCY-SAG14 pair of phytocyanins located on the endomembrane. We also found that PCY-SAG14, which is modulated by PIF3/4/5 and miR408, is both necessary and sufficient to promote senescence. These findings indicate that intracellular copper homeostasis mediated by the PCY-SAG14 module plays an important regulatory role in dark-induced leaf senescence.

[1]To whom correspondence may be addressed. Email: deng@pku.edu.cn or lei.li@pku.edu.cn.

potential role in regulating leaf senescence. Yet this potential mechanism has not been vigorously investigated.

Prolonged darkness causes phenotypes and transcriptome changes largely resembling those during natural senescence (7, 21). Dark-induced senescence (DIS) is therefore used as a simple and efficient system to evaluate the effects of senescence regulators. In this study, by examining the effects of exogenous copper, profiling the transcriptome in different leaf senescing scenarios, tracking subcellular copper distribution during DIS, and genetic and molecular experiments, we found that copper translocation from plastocyanin to a phytocyanin module on the endomembrane critically underpins DIS in *Arabidopsis*. These findings revealed a regulatory role of copper in leaf senescence that warrants further investigation.

Results

Exogenous Copper Promotes Senescence. Employing DIS of 3-wk-old *Arabidopsis* plants as the experimental system, we found that 3 d after dark incubation (DDI) was sufficient to induce senescence symptoms in the rosette leaves, resulting in significantly reduced chlorophyll level and increased ion leakage (*SI Appendix*, Fig. S1). Because ion leakage is a hallmark of the progression of senescence, we initiated an effort to test whether bivalent metal ions in the leaf could impact senescence by treating light-grown *Arabidopsis* plants with the metals. Here we report that, under otherwise identical conditions, copper induced in a dose-dependent manner visible leaf yellowing (*SI Appendix*, Fig. S2A) and significant reduction of chlorophyll levels in light-grown plants (*SI Appendix*, Fig. S2B), a phenotype similar to that caused by light deprivation (21). This result indicates that exogenously supplied copper promotes leaf senescence and this effect was referred to as copper-induced senescence (CIS).

Healthy chloroplasts have stacked thylakoid membranes separated by stromal lamellae, whereas senescing chloroplasts become rounder in shape, gradually losing membrane folds, and accumulate the densely stained plastoglobuli (22). Using transmission electron microscopy (TEM), we found that both dark and copper treatments caused coalescence of membranes into large loose folds and the accumulation of plastoglobuli (Fig. 1A and *SI Appendix*, Fig. S2C), signs of chloroplast aging (22). Given that the chloroplast is a major copper sink in photosynthetic mesophyll cells (16, 23), we tested whether copper levels in the chloroplasts are altered during DIS and CIS. To this end, we analyzed the distribution of copper at the organelle level using energy-filtered TEM (EF-TEM) (Fig. 1B), which uses the energy loss spectrum to distinguish chemical elements. This analysis revealed that senescing chloroplasts after dark treatment contained significantly less copper than their healthy counterparts (Fig. 1C).

To further track the copper efflux from senescing chloroplasts, we developed a fluorescence assay by employing the fluorescent copper probe coppersensor-3 (CS3) (24, 25). In this assay, individually isolated mesophyll cells from the leaf were stained with CS3 and then subjected to fluorescence microscopy simultaneously with examination of chlorophyll autofluorescence. We found that CS3, but not the control probe Ctrl-CS3 with the identical BODIPY fluorophore but lacks copper-binding affinity (*SI Appendix*, Fig. S3A) (25), produced substantial signals that superimposed with the chlorophyll autofluorescence (*SI Appendix*, Fig. S3 B–D). After dark treatment, we observed a reduction in the chloroplast copper content that paralleled a decline of chlorophylls (Fig. 1D and *SI Appendix*, Fig. S3B). In high copper–treated leaves, quantification of fluorescence intensity confirmed parallel reduction of the CS3 fluorescence and chlorophyll autofluorescence (*SI Appendix*, Fig. S4). Together, these results indicate that similar changes occur to the chloroplast during DIS and CIS.

Parallel Transcriptomic Changes Are Elicited in CIS and DIS. We utilized available RNA-sequencing (RNA-Seq) data documenting transcriptome changes caused by darkness or excess copper to further compare DIS and CIS. We identified 1,840 differentially expressed genes (DEGs) common in DIS and CIS, including 315 commonly up-regulated and 1,069 commonly down-
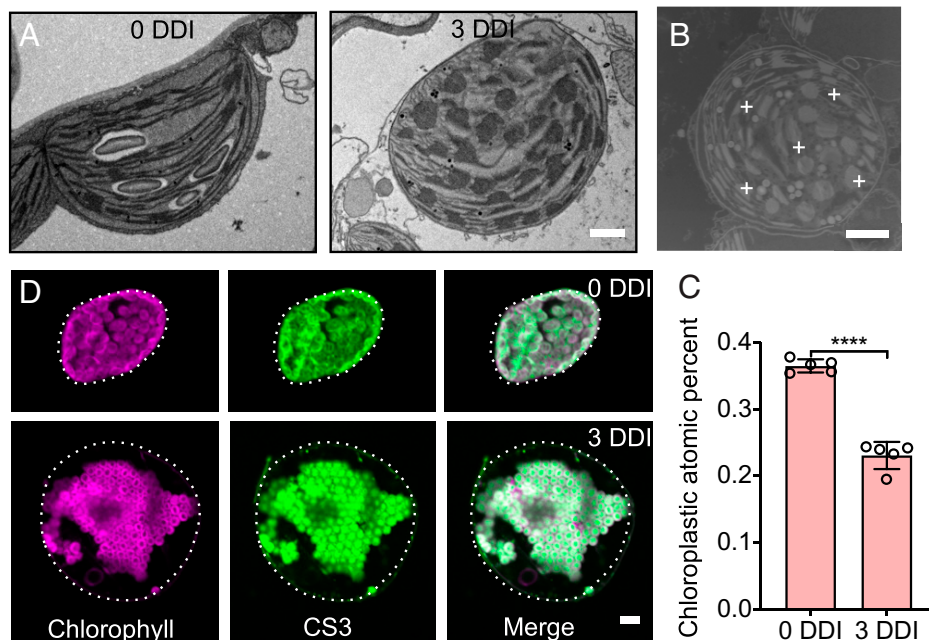
Fig. 1. Examination of the chloroplast in DIS. (*A*) TEM images showing chloroplast ultrastructure at 0 and 3 DDI. (Scale bar, 1 μm.) (*B*) Representative image in the EF-TEM analysis of the chloroplast. Cross marks indicate the collected data points. (Scale bar, 1 μm.) (*C*) Average copper levels in the leaf chloroplast at 0 and 3 DDI determined by EF-TEM. Data are mean ± SD ($n = 5$ independent biological samples). ****$P < 0.0001$ by Student's t test. (*D*) Copper and chlorophyll accumulation pattern in individual mesophyll cells isolated from 0 and 3 DDI leaves. Cells were stained with CS3 and subjected to fluorescence microscopy analysis. (Scale bar, 10 μm.)

Hao et al.
The PCY-SAG14 phytocyanin module regulated by PIFs and miR408
promotes dark-induced leaf senescence in *Arabidopsis*

regulated genes (*SI Appendix*, Fig. S5*A*). Both clustering (*SI Appendix*, Fig. S5*B*) and Pearson correlation analyses (*SI Appendix*, Fig. S5*C*) further revealed that these common DEGs exhibited a high correlation in DIS and CIS. Progressive loss of chlorophyll and reduction of photosynthesis are the hallmarks of leaf senescence. Kyoto Encyclopedia of Genes and Genomes (KEGG) and Gene Ontology (GO) analyses revealed that genes associated with the biosynthesis and degradation of chlorophylls, as well as the photosystems, were enriched in the DEGs common between DIS and CIS (*SI Appendix*, Figs. S6 and S7). Of the 600 identified senescence-related genes in *Arabidopsis* (26), a majority were consistently up- or down-regulated in DIS and CIS (*SI Appendix*, Fig. S8). We selected four genes, three hallmark *SAG*s (*SAG12*, *SAG13*, and *SEN4*), and one gene representative of photosynthesis (*CAB1* encoding chlorophyll A/B binding protein 1), for RT-qPCR analysis. This experiment confirmed the expected expression pattern of the four genes in DIS and CIS (*SI Appendix*, Fig. S9). Collectively, these results indicate that parallel global transcriptomic changes are elicited in DIS and CIS, further supporting a role of copper in regulating leaf senescence.

Copper Reallocation during Senescence. Copper is highly reactive in redox reactions and thus tightly sequestered as a ligand to chaperones and other copper proteins (17, 18, 20). To pinpoint which copper proteins participate in regulating senescence, we adopted the "copper quota" concept, which has been used to describe the cumulative amount of major copper proteins in green algae that is tightly regulated by copper availability and the balance between assimilation and efflux (27). Applying this concept to leaf senescence, we annotated 114 copper binding proteins in *Arabidopsis*, which were divided into six groups according to their known or predicted subcellular locations, including chloroplast, cytoplasm, nucleus, mitochondrion, apoplast, and endomembrane (Fig. 2*A* and Dataset S1). We utilized five gene expression datasets documenting transcriptomic changes in four senescing scenarios, including DIS, CIS, naturally occurring senescence (NOS), and dark-induced senescence of attached leaf (referred to as DAS) (26, 28), to track changes in the copper quota. We estimated the copper quota of different cellular compartments by calculating the accumulated transcript abundance of the representative copper proteins (27). We found that the chloroplast, cytoplasm, and endomembrane have higher copper quotas than the other compartments (Fig. 2*A*). During the process of senescence, a profound decline in the copper quota in the chloroplast concurrent with the increased copper quota in the endomembrane was observed (Fig. 2*A*). This shift in the copper quota occurred prior to or no later than the onset of visible senescence phenotypes (Fig. 2*A*). Consistent with analyses of chloroplastic copper (Fig. 1 and *SI Appendix*, Figs. S3 and S4), these results indicate that copper translocation from the chloroplast to the endomembrane compartment is a common thread in different leaf senescing scenarios.

In the chloroplast, plastocyanin (encoded by *PETE2* in *Arabidopsis*) is the dominant copper protein containing a characteristic mononuclear type-I copper binding motif (29, 30) and is drastically down-regulated during senescence (Fig. 2*B* and *SI Appendix*, Fig. S10 *A–C*). In the endomembrane compartment, most copper
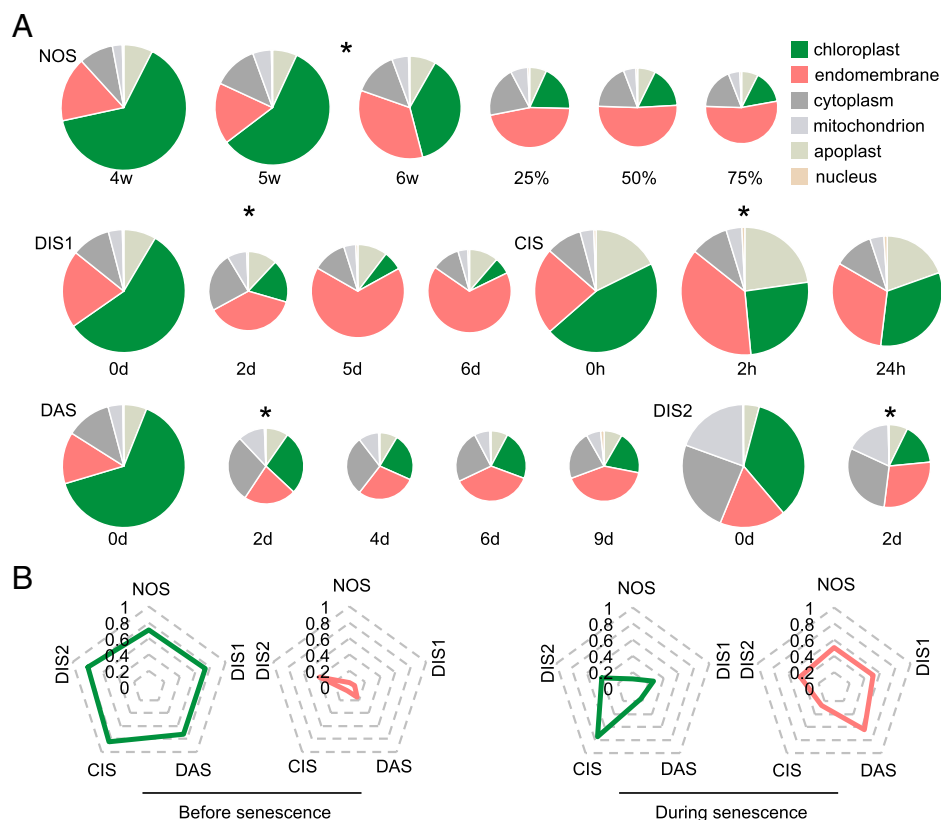
Fig. 2. Reciprocal regulation of chloroplast and endomembrane copper proteins underlies different leaf senescence scenarios. (*A*) Annotated copper binding proteins in *Arabidopsis* were divided into six groups based on their predicted subcellular localizations. Pie graphs indicate the accumulative transcript levels of the copper proteins assigned to each compartment under different senescence scenarios: 4 wk, 5 wk, and 6 wk, age (in weeks) of the plants in NOS; 25%, 50%, and 75%, extents by which senescence was accomplished during NOS according to ref. 27. Numbers in other senescence scenarios indicate time after the treatments were applied. Asterisks indicate the time point at which symptoms of senescence begin to appear. (*B*) Radar plots showing the expression patterns of representative cuproproteins in the chloroplast (plastocyanin in green) and on the endomembrane (SAG14 and PCY in pink) before (*Left*) and during (*Right*) senescence.

Hao et al.
The PCY-SAG14 phytocyanin module regulated by PIFs and miR408 promotes dark-induced leaf senescence in *Arabidopsis*

PNAS | 3 of 10
https://doi.org/10.1073/pnas.2116623119

proteins also contain the plastocyanin-like or phytocyanin domain (Dataset S1). The most conspicuous senescence-related endomembrane phytocyanin gene is *SAG14*, which has long been recognized as a major *SAG* that is robustly induced upon dark adaptation and other stress conditions (31–33). Similarly, plantacyanin (PCY) is a member of the phytocyanin family and has been implicated in pollen tube growth and seed germination (30, 34). We found that *SAG14* and *PCY* exhibit strong concurrent expression during the progression of senescence and eventually account for almost half of the copper quota of the endomembrane (Fig. 2*B* and *SI Appendix*, Fig. S10 *A–C*). The reciprocal accumulation pattern of plastocyanin and *PCY-SAG14* in DIS was confirmed by RT-qPCR analysis (*SI Appendix*, Fig. S10*D*). These results revealed the PCY-SAG14 phytocyanin pair as a candidate in regulating leaf senescence.

SAG14 and PCY Form an Endomembrane Phytocyanin Module. Both PCY and SAG14 are compact proteins that contain only the type-I copper motif and predicted transmembrane motifs (*SI Appendix*, Fig. S11*A*), suggesting that subcellular localization is important for their function. We used a transient expression assay to confirm the endomembrane localization of PCY and SAG14. We generated the *35S:SAG14-GFP* and *35S:PCY-mCherry* reporters, in which SAG14 and PCY, respectively, were fused in-frame to the green fluorescent protein (GFP) and mCherry driven by the constitutive *35S* promoter. We found that both SAG14-GFP and PCY-mCherry transiently expressed in tobacco leaf epidermal cells predominantly localized on the endomembrane (*SI Appendix*, Fig. S11*B*). Furthermore, coexpression of SAG14-GFP and PCY-mCherry in the same cells revealed significant colocalization of the two phytocyanins on the membrane (*SI Appendix*, Fig. S11 *C* and *D*).

To test whether the two phytocyanins interact with each other, we performed a firefly luciferase (LUC) complementation imaging assay by fusing PCY and SAG14 to the C-terminal and N-terminal portions of LUC, respectively. As shown in *SI Appendix*, Fig. S11*E*, coexpression of cLUC-PCY and SAG14-nLUC resulted in robust LUC luminescence. However, the cLUC-PCY plus nLUC and SAG14-nLUC plus cLUC combinations did not show LUC complementation, indicating that SAG14 specifically interacts with PCY. These results together with the concurrent expression pattern during senescence indicate that PCY and SAG14 form a phytocyanin module on the endomembrane for regulating senescence.

The PCY-SAG14 Module Enhances DIS. To genetically determine the role of PCY-SAG14 in leaf senescence, we used the reported T-DNA insertion line (*pcy-1*) and CRISPR-Cas9 knockout line (*pcy-ko*) disrupting *PCY* (30) for phenotypic analysis. Compared to the wild type, leaf yellowing of *pcy-1* and *pcy-ko* was significantly delayed (Fig. 3*A* and *SI Appendix*, Fig. S12*A*), chlorophyll contents remained significantly higher (Fig. 3*B* and *SI Appendix*, Fig. S12*B*), and ion leakage was significantly reduced during DIS (Fig. 3*C* and *SI Appendix*, Fig. S12*C*). In contrast, overexpression of PCY driven by the *35S* promoter (*35S:PCY*) in *Arabidopsis* accelerated the presentation of DIS symptoms, judging from the visibility of leaf yellowing, chlorophyll content, and ion leakage (Fig. 3 *A–C* and *SI Appendix*, Fig. S12 *A–C*). Next, we utilized two independent T-DNA insertion lines (*sag14-1* and *sag14-2*) disrupting *SAG14* for phenotypic analysis. Compared to the wild type, the *sag14-1* and *sag14-2* leaves exhibited significantly delayed yellowing, higher chlorophyll contents, and lower ion leakage, whereas the DIS phenotypes of the *35S:SAG14* overexpression lines exhibited the opposite (*SI Appendix*, Fig. S13 *A–C*). These results established that both *PCY* and *SAG14* are positive regulators of DIS.

TEM analysis showed that both the *pcy* and *sag14* mutants maintained better-preserved membrane structures in the

chloroplast than the wild type experiencing the same period of dark treatment (Fig. 3*E* and *SI Appendix*, Fig. S13*D*), indicating that chloroplast dismantling was delayed in the mutants. Further analysis by EF-TEM revealed that chloroplast copper levels in *pcy* and *PCY-OX* were significantly higher and lower, respectively, compared to the wild type after dark treatment (Fig. 3*D*). Examination of copper levels in isolated mesophyll cells using the CS3 staining assay revealed a slower than wild type decline in chloroplast copper after darkness in *pcy* and *sag14*, whereas the *PCY-OX* and *SAG14-OX* overexpression lines exhibited opposite phenotypes from the mutants (Fig. 3*F* and *SI Appendix*, Fig. S13*E*). Collectively, these results indicate that PCY-SAG14 is required for promoting DIS by facilitating intracellular copper redistribution.

miR408 Retards Senescence by Repressing PCY-SAG14. In examining how the PCY-SAG14 module is regulated, we noticed that *PCY* is a proven target for miR408, a microRNA conserved in land plants (19, 35). We employed *miR408-OX* and *STTM408* transgenic plants, in which miR408 is overexpressed driven by the *35S* promoter (36) and silenced by a short tandem target mimic (30), respectively. We found that the expression levels of *PCY* and *SAG14* were significantly reduced in *miR408-OX* but increased in *STTM408* compared to the wild-type plants (*SI Appendix*, Fig. S14). Moreover, DIS was significantly retarded in *miR408-OX* but accelerated in *STTM408* in comparison to the wild type, as indicated by leaf yellowing, chlorophyll level, and the degree of ion leakage (Fig. 4 *A–C*). These results indicate that miR408 negatively regulates DIS by repressing expression of the PCY-SAG14 module.

To test whether miR408 influences the chloroplast-to-endomembrane copper translocation in DIS, we performed TEM, EF-TEM, and CS3 staining analyses. We found that chloroplast morphology and copper content were better preserved in *miR408-OX* but more deteriorated in *STTM408* compared to the wild-type leaf experiencing the same length of darkness (Fig. 4 *D–F*). Thus, consistent with previous reports that miR408 promotes copper allocation to the chloroplast and enhances plastocyanin abundance (35, 37), our results indicate that miR408 retards senescence by hindering chloroplast copper efflux to the PCY-SAG14 module.

In line with its role in hindering senescence, we found that miR408 expression level determined by RT-qPCR analysis was drastically decreased under various senescence conditions, including DIS, CIS, and NOS (*SI Appendix*, Fig. S15*A*). Using *Arabidopsis* reporter lines expressing *pMIR408:GUS*, in which the *β-glucuronidase* (*GUS*) gene is driven by the *MIR408* promoter (36), or *pMIR408:LUC*, we found that the *MIR408* promoter was suppressed by dark and copper treatments (*SI Appendix*, Fig. S15 *B–D*). These results indicate that miR408-based regulation of the PCY-SAG14 module coordinates with PCY-SAG14–mediated copper translocation during senescence.

PIF3/4/5 Regulates Copper Translocation in DIS by Repressing miR408. Phytochrome-interacting factors (PIFs) are transcription factors that regulate various light responses, and the PIF3/4/5 trio is key to promoting DIS (38, 39). Therefore, we tested whether PIF3/4/5 regulates copper translocation to PCY-SAG14. This inquiry was facilitated by available whole-genome chromatin immunoprecipitation (ChIP) data (40–42) that revealed specific PIF3/4/5 occupancy at a G-box motif in the *MIR408* proximal promoter (Fig. 5*A*). This observation was corroborated by ChIP-qPCR analysis using transgenic plants overexpressing MYC-tagged PIF3/4/5 (43), which showed more enriched binding to the *MIR408* promoter than in the wild type (Fig. 5*B*). These results validated that PIF3/4/5 directly binds to the *MIR408* promoter.
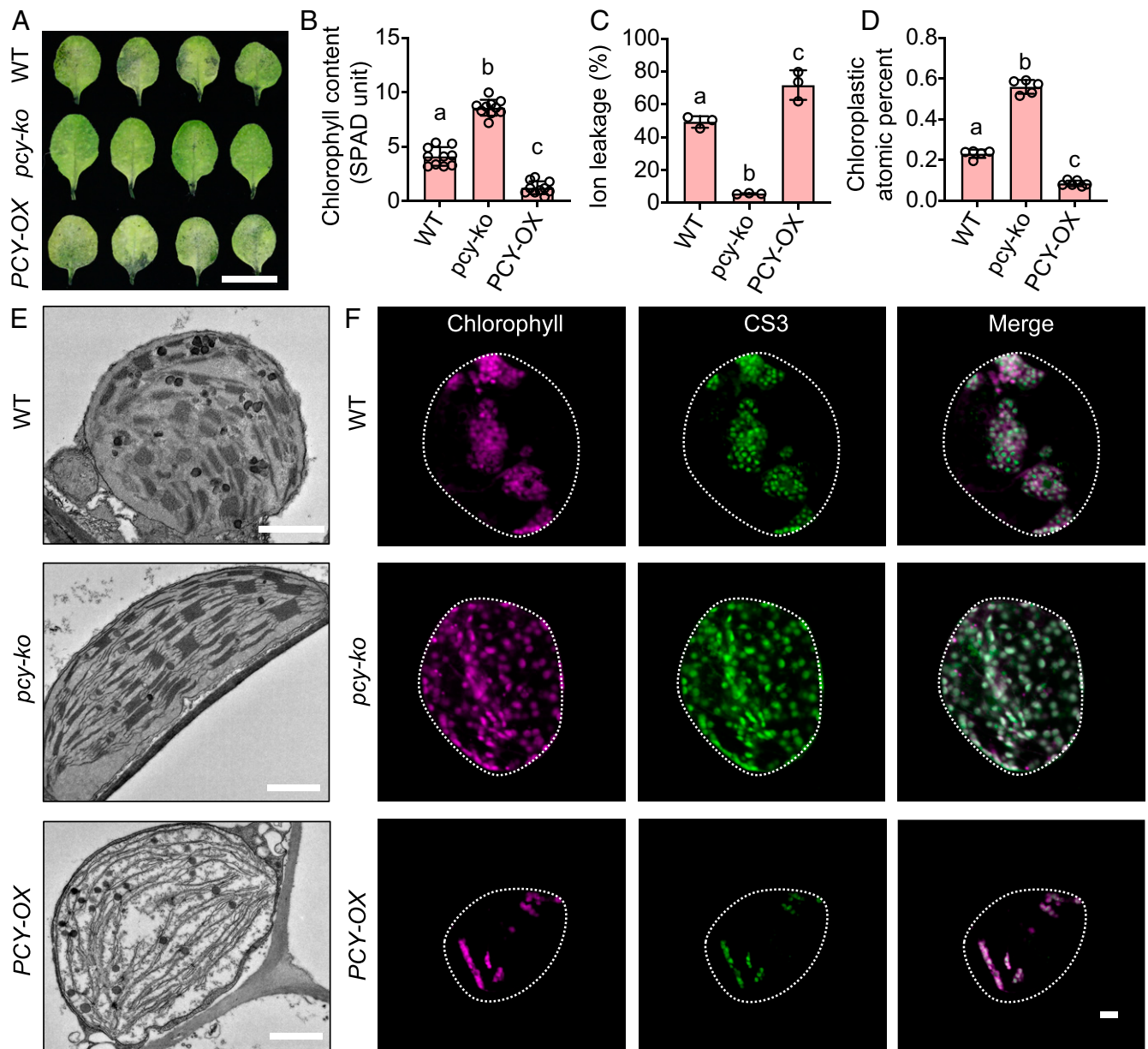
Fig. 3. PCY promotes DIS. (*A*) Leaves of the *pcy-ko*, *PCY-OX*, and wild-type plants at 3 DDI. (Scale bar, 1 cm.) (*B–D*) Quantitative measurement of chlorophyll contents (in SPAD unit) (*B*), ion leakage (*C*), and chloroplast copper contents (*D*) in leaves shown in *A*. Data are mean ± SD ($n = 10$ for *B*, $n = 3$ for *C*, and $n = 6$ for *D*, independent biological samples). Different letters denote genotypes with significant differences (ANOVA, $P < 0.01$). (*E*) TEM images showing chloroplast ultrastructures of the three indicated genotypes at 3 DDI. (Scale bars, 1 μm.) (*F*) Copper and chlorophyll accumulation pattern in individual mesophyll cells isolated from 3 DDI leaves of the three indicated genotypes. Cells were stained with CS3 and subjected to fluorescence microscopy analysis. WT, wild type. (Scale bar, 10 μm.)

Using the *pMIR408:LUC* reporter, we observed that LUC activity was significantly weakened when coexpressed in tobacco leaf epidermal cells with either *PIF4* or *PIF5* (Fig. 5 *C* and *D*). When the G box in the *MIR408* promoter was mutated, the effect of PIF4/5 on *pMIR408:LUC* was no longer observed (Fig. 5 *E* and *F*). As a control, elongated hypocotyl 5 (HY5), which is a known positive regulator of miR408 (37), increased LUC activity when coexpressed with *pMIR408:LUC* (*SI Appendix,* Fig. S16). These results indicate that PIF4/5 inhibits the *MIR408* promoter in a G-box–dependent manner. To confirm this inhibitory effect in *Arabidopsis*, we employed the *pMIR408: GUS* plants and crossed the *pMIR408:GUS* reporter gene into the *pif4*, *pif5*, and *pifq* (a *PIF1/3/4/5* quadruple mutant) (44) background (*SI Appendix,* Fig. S17*A*). We found that etiolated

seedlings of *pMIR408:GUS/pif4*, *pMIR408:GUS/pif5*, and *pMIR408:GUS/pifq* exhibited higher GUS activities than *pMIR408:GUS* (*SI Appendix,* Fig. S17*A*). Consistently, we found that the miR408 transcript level was increased in the *pif4*, *pif5*, and *pifq* mutants but decreased in *PIF4-MYC* and *PIF5-MYC* compared to wild type (*SI Appendix,* Fig. S17 *B* and *C*). Collectively, these results indicate that PIF3/4/5 represses miR408 by directly binding to its promoter.

Phenotypically, we confirmed that the *pifq* mutant exhibited drastically retarded DIS compared to wild type (38), based on leaf yellowing, chlorophyll level, and the degree of ion leakage (Fig. 4 *A–C*). Using TEM, EF-TEM, and CS3 staining analyses, we found that chloroplast morphology was better preserved in *pifq* and more copper retained in the *pifq* chloroplast compared
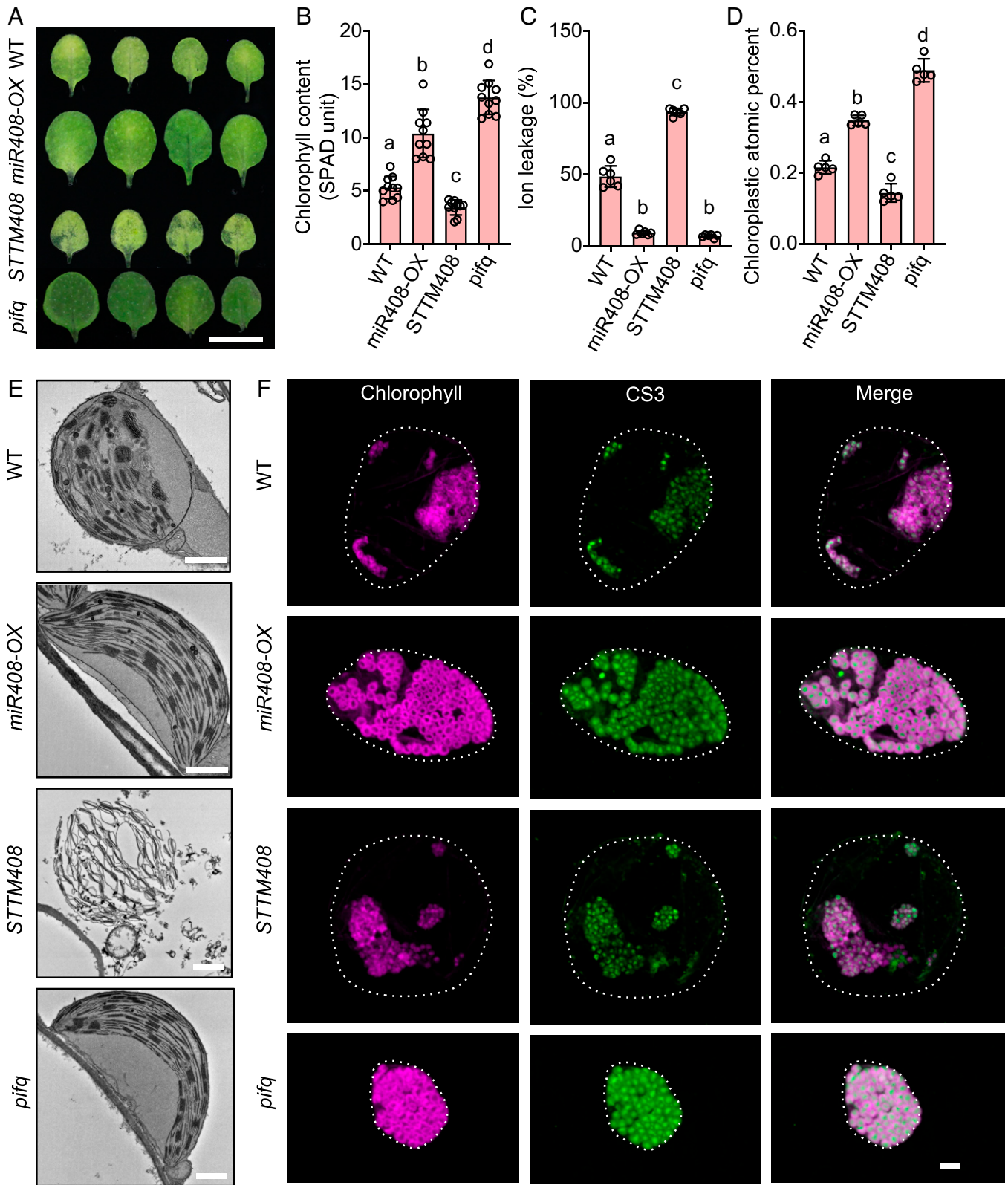
Hao et al.
The PCY-SAG14 phytocyanin module regulated by PIFs and miR408
promotes dark-induced leaf senescence in *Arabidopsis*

PNAS | 5 of 10
https://doi.org/10.1073/pnas.2116623119

Fig. 4. miR408 and PIFs play opposite roles in regulating DIS. (*A*) Leaves of the *miR408-OX*, *STTM408*, *pifq*, and wild-type plants at 3 DDI. (Scale bar, 1 cm.) (*B–D*) Quantitative measurement of chlorophyll contents (in SPAD unit) (*B*), ion leakage (*C*), and chloroplast copper contents (*D*) in leaves shown in *A*. Data are mean ± SD (*n* = 10 for *B*, *n* = 3 for *C*, and *n* = 6 for *D*, independent biological samples). Different letters denote genotypes with significant differences (ANOVA, *P* < 0.01). (*E*) TEM images showing chloroplast ultrastructures of the four indicated genotypes at 3 DDI. (Scale bars, 1 μm.) (*F*) Copper and chlorophyll accumulation pattern in individual mesophyll cells isolated from 3 DDI leaves of the four indicated genotypes. Cells were stained with CS3 and subjected to fluorescence microscopy analysis. (Scale bar, 10 μm.)
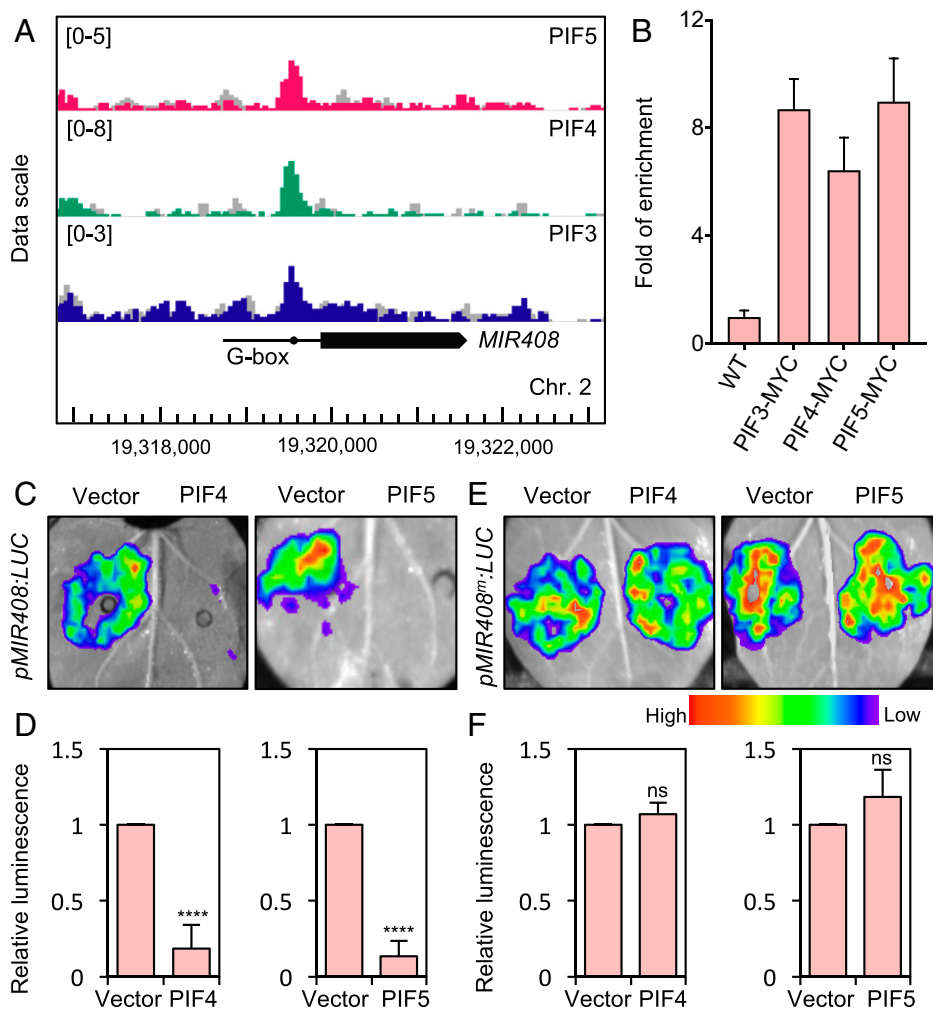
Hao et al.
The PCY-SAG14 phytocyanin module regulated by PIFs and miR408
promotes dark-induced leaf senescence in *Arabidopsis*

Fig. 5. PIF3/4/5 directly inhibits miR408 expression. (*A*) PIF3/4/5 binding pattern at the *MIR408* locus based on ChIP-Seq data. Positions of *MIR408* and its proximal promoter region are depicted as a black arrow and a horizontal line, respectively. Dot in the promoter region represents the G-box–like motif. (*B*) Confirmation of PIF3/4/5 binding to the *MIR408* promoter by ChIP-qPCR analysis. ChIP was performed on etiolated seedlings of the indicated genotypes using the anti-MYC antibody. Data are mean ± SD (*n* = 3 independent qPCR performed on the same DNA). (*C* and *D*) Transient expression assay in tobacco epidermal cells showing the effect of PIF4 and PIF5 on LUC activity driven by the *MIR408* promoter. Representative images are shown in *C*. Quantification of relative luminescence is shown in *D*. Data are mean ± SD (*n* = 15 independent biological samples). ****$P < 0.0001$ by Student's *t* test. (*E* and *F*) Transient expression assay showing the effect of PIF4 and PIF5 on LUC activity driven by the *MIR408* promoter with the G box mutated. Representative images are shown in *E*. Quantification of relative luminescence is shown in *F*. Data are mean ± SD (*n* = 15 independent biological samples). ns, not significant by Student's *t* test.

to the wild type experiencing the same length of darkness (Fig. 4 *D–F*). Taken together, these results indicate that PIF3/4/5-miR408–based regulation of PCY-SAG14 in the nucleocytoplasm space coordinates with PCY-SAG14–mediated copper translocation to the endomembrane to regulate DIS (Fig. 6).

Discussion

In this study, using DIS as the experimental system, we found that copper homeostasis regulates senescence based on several lines of evidence. First, we showed that exogenous copper could induce the senescence syndrome and transcriptomic changes in light-grown plants parallel to those elicited in DIS (Fig. 1 and *SI Appendix*, Figs. S1–S5). Second, we identified reciprocal regulation of small blue copper proteins, plastocyanin in the chloroplast, and PCY-SAG14 on the endomembrane, as a common trend in different leaf senescing scenarios (Fig. 2). Third, genetic and molecular experiments demonstrated that the PCY-SAG14 module was necessary and sufficient for the promotion of DIS (Fig. 3 and *SI Appendix*, Figs. S12 and S13). Finally, we showed that PCY-SAG14 was regulated by miR408

and PIF3/4/5 (Figs. 4 and 5), indicating that subcellular copper redistribution during DIS is coordinated with gene regulation in the nucleocytoplasm space (Fig. 6). Overall, these findings support chloroplast-to-endomembrane copper translocation modulated by the PIF-miR408 circuit as a regulator of DIS in *Arabidopsis*. It is noteworthy that both the PIF-miR408 circuit and the small blue copper proteins are conserved in land plants (19, 30, 31, 35), suggesting that regulated copper redistribution during DIS is an evolutionarily conserved mechanism.

Although many molecular and physiological details remain to be elucidated, a role of copper in regulating senescence is consistent with our current understanding of leaf function and development. First, as the driver of photosynthesis in green plants, photosynthetic electron transport is sensitive to aging and environmental perturbations (45). This entails that copper emanated from the turnover of plastocyanin, the indispensable mobile electron carrier in the electron transport chain and the main copper protein in the chloroplast (14–16), could serve as an indicator for the state of the chloroplasts. Second, copper remobilized from plastocyanin has the capability to respond to and the potential to translate multiple primary cues into an
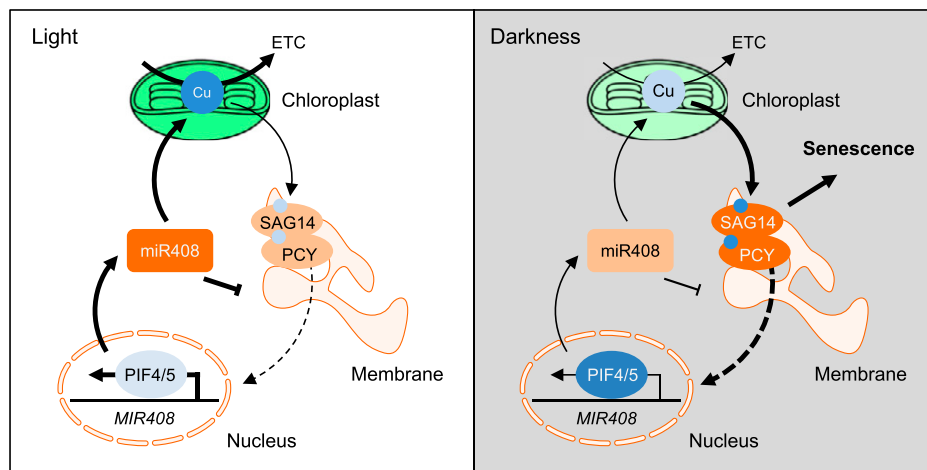
Hao et al.
The PCY-SAG14 phytocyanin module regulated by PIFs and miR408 promotes dark-induced leaf senescence in *Arabidopsis*

PNAS | 7 of 10
https://doi.org/10.1073/pnas.2116623119

Fig. 6. Model of intracellular copper redistribution modulated by PIF-miR408 in regulating DIS. In light, the activated photosynthetic electron transport chain (ETC) keeps copper to the mobile electron carrier plastocyanin in the chloroplast. In the nucleocytoplasm space, disabled PIF3/4/5 allows miR408 to accumulate, which in turn represses the PCY-SAG14 module on the endomembrane. After prolonged darkness, activation of PIF3/4/5 and repression of miR408 in the nucleocytoplasm space facilitate copper translocation from deteriorating plastocyanin, due to blocked ETC, to PCY-SAG14, which in turn promotes senescence.

integrated universal signal for initiating senescence (Fig. 2). Third, different from other transition metals, cellular copper is tightly sequestered in the cytosol (17, 18) and, thus, likely has the required specificity for relaying senescence signaling, which is supported by the finding that exogenously supplied copper was able to promote senescence parallel to DIS. Finally, the subcellular copper quota is tightly regulated by the elaborate copper transport route and cellular homeostasis mechanisms (19, 20, 27), allowing the amount of remobilized copper to carry quantitative information that reflects the chloroplast state for proper regulation of senescence.

Copper is a micronutrient essential for reproduction and seed development (30, 46). Remobilized copper from senescing leaves is exported to sink organs such as new leaves and seeds (47). Notably, copper signaling involving chloroplast-to-endomembrane translocation is a rapid intracellular movement. We found that this translocation might occur prior to or no later than the onset of visible senescence phenotypes based on the transcriptome profiles (Fig. 2*A*). During DIS, we showed that the copper translocation was tightly regulated by light signaling, mediated by PIF3/4/5 and miR408 operating in the nucleocytoplasm space (Figs. 4–6). Therefore, the intracellular signaling role of copper may be separable from the intercellular translocation of copper as a mineral nutrient to sink or reproductive organs during the later stages of senescence.

How does intracellular copper redistribution lead to changes in gene expression that underlie the senescence syndrome? Despite our knowledge of the conserved copper responsive transcription factor SPL7 (squamosa promoter binding protein-like 7) in regulating copper scavenging (37, 48, 49), we know little about the perception and transduction mechanisms of the copper signal. In this study, we identified the PCY-SAG14 phytocyanin pair on the endomembrane that was necessary for chloroplast copper efflux and symptom manifestation during senescence (Fig. 3 and *SI Appendix*, Fig. S13). It is intriguing to note that the perception of ethylene, a major senescence-promoting hormone (6, 26, 50), requires a family of cuproprotein receptors represented by ethylene response 1 (ETR1) and the copper transporter responsive to antagonist 1 (RAN1), which both localize on the endomembrane (51–53). It is possible that the endomembrane PCY-SAG14 module relays the copper signal to RAN1 and/or ETR1 to activate the ethylene signaling pathway, which coordinates with other signaling pathways to ensure proper senescence. Further elucidation of how the PCY-SAG14 module is regulated during aging and how it interfaces with ethylene signaling should provide insights in the understanding of leaf senescence.

Materials and Methods

Plant Materials. The wild-type plants used in this study were *Arabidopsis thaliana* ecotype Col-0. The *pMIR408:LUC*, *pMIR408:GUS*, *miR408-OX*, *STTM408*, *pcy-ko*, *PIF3/4/5-MYC*, *pif4*, *pif5*, and *pifq* plants were described previously (30, 36, 37, 43, 44). The *pcy-1*, *sag14-1*, and *sag14-2* mutants were T-DNA insertion lines obtained from the Nottingham Arabidopsis Stock Centre. The *pMIR408:-GUS* plants were crossed with *pif4*, *pif5*, or *pifq* to generate the *pMIR408:GUS/pif4*, *pMIR408:GUS/pif5*, and *pMIR408:GUS/pifq* plants. The *PCY-OX* and *SAG14-OX* constructs were generated by individually cloning the full-length coding region of PCY and SAG14 into the *pJIM19-GFP* vector in-frame with GFP between the *XbaI* and *XhoI* sites. The *PCY-OX* and *SAG14-OX* constructs were used to transform *Arabidopsis* plants. Homozygous transformants were selected by hygromycin resistance and genotyped in the T_3 population. Two independent homozygous lines were selected for subsequent analyses. The primers used for cloning and genotyping are listed in *SI Appendix*, Table S1. The corresponding sequence data for relevant genes can be found in the *Arabidopsis* Genome Initiative with the following accession nos.: PCY (At2g02850), SAG14 (At5g20230), MIR408 (At2g47015), PIF3 (At1g09530), PIF4 (At1g09530), PIF5 (At3g59060), HY5 (At5g11206), SAG12 (At5g45890), SAG13 (At2g29350), PETE2 (At1g20340), CAB1 (At1g29930), and SEN4 (At4g30270).

Plant Growth and Treatment Conditions. To grow *Arabidopsis* plants, surface sterilized seeds were vernalized on agar-solidified half-strength Murashige and Skoog media containing 1% (wt/vol) sucrose. $CuSO_4$ (Sigma-Aldrich) was supplemented to the indicated final concentrations. Plants were grown under the conditions of 16 h light/8 h dark at 22 °C/20 °C with ~50% relative humidity for 3 wk. Light was provided by white fluorescent bulbs with intensity of ~100 μmol m^{-2} s^{-1}. For DIS-related analysis, the third or fourth rosette leaves were detached and transferred to complete darkness for the indicated periods. Transient assays were performed on tobacco (*Nicotiana benthamiana*) plants, which were maintained in a growth chamber under a 16-h light/8-h dark cycle at 25 °C/21 °C in ~50% relative humidity with a light intensity of ~150 μmol m^{-2} s^{-1}.

Measurement of Chlorophyll Content. Chlorophylls were extracted with 80% (vol/vol) acetone containing 0.1% NH_3 at room temperature in darkness as previously described (30). Absorbance of the supernatant was measured at 645 and 663 nm using NanoPhotometer (Implen). Chlorophyll contents were calculated and normalized to per gram of fresh weight. The chlorophyll contents in individual leaves were also measured using a SPAD-502 Plus chlorophyll meter (Konica Minolta). Each leaf was measured five times at five evenly distributed spots on one blade. The average value of the measurements

Hao et al.
The PCY-SAG14 phytocyanin module regulated by PIFs and miR408
promotes dark-induced leaf senescence in *Arabidopsis*

(SPAD unit) represents a single data point. At least 10 individual leaves were measured and recorded for each genotype.

Measurement of Ion Leakage. Ion leakage was measured as previously described (54, 55). For each sample, approximately five detached rosette leaves from adult plants were incubated in 20 mL of double-distilled water at room temperature for 3 h with gentle shaking. The conductivity of this incubated solution, denoted as C1, was measured using an LE703 conductivity meter (Mettler Toledo). The sample was boiled for 10 min and then cooled to room temperature. The conductivity of the supernatant, denoted as C2, was measured. The degree of ion leakage was calculated as the C1/C2 ratio.

Chemical Synthesis of CS3 and Ctrl-CS3. The CS3 and Ctrl-CS3 probes were custom synthesized as previously described. Briefly, CS1 and Ctrl-CS1 were first chemically synthesized (56), which was then modified via chemical processing as described (25). Afterward, the organic phases were extracted, dried over Na_2SO_4, concentrated under low pressure, and purified with 100% ethyl acetate via flash chromatography. The products were confirmed by ^1H NMR analysis as described (24).

Tracking Cellular Copper by CS3 Staining. The rosette leaves from 3-wk-old plants were fixed in 1 mL of 3.5% glutaraldehyde solution (Sigma-Aldrich) in a tissue culture plate under vacuum for 30 min and then in the dark at 4 °C overnight. After washing away glutaraldehyde, the fixed tissues were incubated in 1 mL of 0.1 M ethylenediaminetetraacetic acid (EDTA) at 65 °C for 20 min. After washing with double-distilled water and cooling to room temperature, the tissues were transferred to a glass slide, covered with 50 to 100 μL of 10 μM CS3 or Ctrl-CS3, and stained at room temperature for 30 min in the dark. Following washing, a cover slide was added and gently pressed to release single mesophyll cells. Fluorescence signals in the single cells were analyzed using a LSM700 confocal laser scanning microscope (Zeiss). The fluorescence of CS3/Ctrl-CS3 and chlorophyll autofluorescence were observed with excitation at 543 nm and 633 nm and emission at 550 to 630 nm and 640 to 730 nm, respectively.

TEM and EF-TEM. The plant samples were fixed first in fixation buffer I (5% glutaraldehyde and 0.1 M phosphate, pH 7.4) for 4 h at room temperature and then in fixation buffer II (2% osmium tetroxide and 0.1 M phosphate, pH 7.4) at 4 °C overnight. After one wash in phosphate buffer and two washes in double-distilled water, the samples were stained for 1 h in 1% (m/v) uranyl acetate. After another wash in double-distilled water, the samples were dehydrated through a gradient of alcohol (from 30%, 50%, 70%, to 85%) and then embedded in Spurr's resin (Sigma-Aldrich). Ultrathin sections of 70 nm were prepared using the UC7 μLtramicrotome (Leica Microsystem) and mounted on the AG100M molybdenum grids with a single slot (Agar Scientific) to minimize the background for copper. The sections were stained with uranyl acetate and lead citrate, observed, and photographed using a Tecnai G2 20 Twin electron microscope (FEI) at 120 kV. EF-TEM for copper element analysis was carried out on the same specimen using a JEM-2100F field-emission high-resolution transmission electron microscope equipped with the energy filter (JEOL). Three individual leaves were used for each genotype and at least 10 cells were analyzed per sample.

Transcriptome Analyses. Raw RNA-Seq data were obtained from the National Center for Biotechnology Information (NCBI) BioProject database (https://www.ncbi.nlm.nih.gov/bioproject/) with the accession nos. PRJNA350795 and PRJEB27631. Quality control was conducted using fastQC (https://www.bioinformatics.babraham.ac.uk/projects/fastqc/) and MultiQC (57). Cutadapt (https://cutadapt.readthedocs.io/en/stable/index.html) was used to trim adaptors. The clean reads were mapped to the TAIR10 *Arabidopsis* genome build using HISAT2. The transcripts in each sample were assembled and quantified using StringTie (58). The outputs from StringTie were processed using the DESeq2 package (59) in R (https://www.r-project.org) to identify differentially expressed genes. Clustering and correlation analyses were performed and visualized using the R packages. GO enrichment analysis was carried out using the clusterProfiler package in R and AgriGO (http://bioinfo.cau.edu.cn/agriGO/). The pheatmap package in R was used to construct heat maps. Processed microarray data were described previously (26).

RT-qPCR Analysis. Total RNA was extracted from plant samples using the Quick RNA Isolation Kit (Huayueyang). First-strand cDNA for mRNA and miRNA was generated using the PrimeScript II First Strand cDNA Synthesis Kit

(TaKaRa) and the miRcute Plus miRNA First-Stand cDNA Synthesis Kit (Tiangen), respectively. Quantitative PCR analysis was performed using the SYBR Green Mix (TaKaRa) on the 7500 Fast Real-Time PCR System (Applied Biosystems). Relative transcript abundance was determined by the comparative threshold cycle method. *GADPH* and 5S RNA were used for mRNA and miRNA normalization, respectively. The sequences of the primers are listed in *SI Appendix*, Table S1.

ChIP Analyses. The original ChIP-Seq data for PIFs were described in previous studies (40–42) and obtained from the NCBI Gene Expression Omnibus database (https://www.ncbi.nlm.nih.gov/geo) with the accession numbers GSE39215, GSE35315, and GSE35059. Quality control was conducted using fastQC (https://www.bioinformatics.babraham.ac.uk/projects/fastqc/) and MultiQC (57). Trim Galore (https://www.bioinformatics.babraham.ac.uk/projects/trim_galore/) was used to remove low-quality bases and to trim adaptor sequences. The clean reads were mapped to the *Arabidopsis* genome using Bowtie2 (60). MACS2 (https://macs3-project.github.io/MACS/) was used to call peaks and the peaks were visualized using DeepTools (61) and the Integrative Genomics Viewer (https://igv.org). To validate PIF3/4/5 binding to the *MIR408* promoter, 4-d-old etiolated *PIF3-MYC*, *PIF4-MYC*, *PIF5-MYC*, and wild-type seedlings were cross-linked in 1% formaldehyde for 30 min under vacuum. ChIP was performed following the procedure previously described (30) using an anti-MYC antibody (Sigma-Aldrich) for immunoprecipitation. After ChIP, an equal amount of input DNA was subjected to qPCR analysis of the target DNA fragment. Fold enrichment was calculated against the wild type.

Histochemical Analysis of GUS Activity. In situ GUS staining of *Arabidopsis* seedlings was performed as described previously (36). Briefly, whole seedlings were incubated in GUS staining solution (0.1 M $NaPO_4$, pH 7.0, 10 mM EDTA, 0.1% Triton X-100, 1 mM $K_3Fe(CN)_6$, and 2 mM X-Gluc) at 37 °C overnight. Stained samples were decolorized several times using 75% ethanol until chlorophyll was no longer visible. Representative images of the GUS staining pattern were taken with a digital camera.

LUC Assays. To generate *pMIR408:LUC*, the promoter was PCR amplified from *Arabidopsis* genomic DNA and cloned into the *p1305.1-LUC* vector. The *pJIm19-PIF3*, *pJIm19-PIF4*, *pJIm19-PIF5*, and *pJIM19-HY5* constructs containing the coding sequences of PIF3, PIF4, PIF5, and HY5 were generated using overlap extension PCR and cloned into the *pJIM19* vector. *Agrobacterium* strains harboring the *pJIM19:PIF3/4/5* effectors and the *pMIR408:LUC* reporter were mixed to infiltrate tobacco leaf epidermal cells. After 2 d in darkness at 25 °C, the leaves were detached and sprayed with 20 mg mL^{-1} potassium luciferin (Gold Biotech) and incubated in darkness for 5 min. Luminescence from the infiltrated area was imaged using the NightShade LB 985 system (Berthold). IndiGO software (version 2.03.0) was used to quantitate the luminescence. More than 10 biological repeats were measured per sample and the representative images are shown. For the LUC complementation imaging assay, the coding sequences of SAG14 and PCY were cloned into the *pCAMBIA1300-nLUC* and *pCAMBIA1300-cLUC* vectors, respectively. The *pCAMBIA1300-nLUC* or *pCAMBIA1300-cLUC* vector was used as a control. *Agrobacterium* cells expressing the reporter constructs were used to infiltrate tobacco epidermal cells. After 2 d, the leaves were sprayed with 20 mg mL^{-1} potassium luciferin and luminescence was recorded.

Statistical Analysis. Two-tailed Student's *t* test was used for pairwise comparisons. One-way ANOVA was used to determine significance in multiple comparisons. Tukey's test was used post hoc to compare group means at the indicated significance levels.

Data Availability. All study data are included in the article and/or supporting information. Previously published data were used for this work (raw RNA-Seq data were obtained from the NCBI BioProject database (https://www.ncbi.nlm.nih.gov/bioproject/) under accession nos. PRJNA350795 (62) and PRJEB27631 (28). The original ChIP-Seq data for PIFs were obtained from the NCBI Gene Expression Omnibus database (https://www.ncbi.nlm.nih.gov/geo) under accession nos. GSE39215, GSE35315, and GSE35059 (40–42).

1. P. O. Lim, H. J. Kim, H. G. Nam, Leaf senescence. *Annu. Rev. Plant Biol.* **58**, 115–136 (2007).
2. H. R. Woo, H. J. Kim, P. O. Lim, H. G. Nam, Leaf senescence: Systems and dynamics aspects. *Annu. Rev. Plant Biol.* **70**, 347–376 (2019).
3. Y. Guo et al., Leaf senescence: Progression, regulation, and application. *Molecular Horticulture* **1**, 5 (2021).
4. S. Gan, R. M. Amasino, Inhibition of leaf senescence by autoregulated production of cytokinin. *Science* **270**, 1986–1988 (1995).

PLANT BIOLOGY

5. C. Uauy, A. Distelfeld, T. Fahima, A. Blechl, J. Dubcovsky, A NAC Gene regulating senescence improves grain protein, zinc, and iron content in wheat. *Science* **314**, 1298–1301 (2006).

6. J. H. Kim *et al.*, Trifurcate feed-forward regulation of age-dependent cell death involving miR164 in *Arabidopsis*. *Science* **323**, 1053–1057 (2009).

7. Y. Guo, S.-S. Gan, Convergence and divergence in gene expression profiles induced by leaf senescence and 27 senescence-promoting hormonal, pathological and environmental stress treatments. *Plant Cell Environ.* **35**, 644–655 (2012).

8. Y. Ma *et al.*, COLD1 confers chilling tolerance in rice. *Cell* **160**, 1209–1221 (2015).

9. J.-H. Jung *et al.*, Phytochromes function as thermosensors in *Arabidopsis*. *Science* **354**, 886–889 (2016).

10. N. Dai *et al.*, Overexpression of *Arabidopsis* hexokinase in tomato plants inhibits growth, reduces photosynthesis, and induces rapid senescence. *Plant Cell* **11**, 1253–1266 (1999).

11. B. Moore *et al.*, Role of the *Arabidopsis* glucose sensor HXK1 in nutrient, light, and hormonal signaling. *Science* **300**, 332–336 (2003).

12. F. Rolland, E. Baena-Gonzalez, J. Sheen, Sugar sensing and signaling in plants: Conserved and novel mechanisms. *Annu. Rev. Plant Biol.* **57**, 675–709 (2006).

13. S. Munné-Bosch, L. Alegre, Plant aging increases oxidative stress in chloroplasts. *Planta* **214**, 608–615 (2002).

14. S. Katoh, A new copper protein from *Chlorella ellisoidea*. *Nature* **186**, 533–534 (1960).

15. F. P. Molina-Heredia *et al.*, Photosynthesis: A new function for an old cytochrome? *Nature* **424**, 33–34 (2003).

16. M. Weigel *et al.*, Plastocyanin is indispensable for photosynthetic electron flow in *Arabidopsis thaliana*. *J. Biol. Chem.* **278**, 31286–31289 (2003).

17. T. D. Rae, P. J. Schmidt, R. A. Pufahl, V. C. Culotta, T. V. O'Halloran, Undetectable intracellular free copper: The requirement of a copper chaperone for superoxide dismutase. *Science* **284**, 805–808 (1999).

18. L. A. Finney, T. V. O'Halloran, Transition metal speciation in the cell: Insights from the chemistry of metal ion receptors. *Science* **300**, 931–936 (2003).

19. J. L. Burkhead, K. A. Gogolin Reynolds, S. E. Abdel-Ghany, C. M. Cohu, M. Pilon, Copper homeostasis. *New Phytol.* **182**, 799–816 (2009).

20. N. J. Robinson, D. R. Winge, Copper metallochaperones. *Annu. Rev. Biochem.* **79**, 537–562 (2010).

21. D. Liebsch, O. Keech, Dark-induced leaf senescence: New insights into a complex light-dependent regulatory pathway. *New Phytol.* **212**, 563–570 (2016).

22. I. M. Evans, A. M. Rus, E. M. Belanger, M. Kimoto, J. A. Brusslan, Dismantling of *Arabidopsis thaliana* mesophyll cell chloroplasts during natural leaf senescence. *Plant Biol.* **12**, 1–12 (2010).

23. P. Pesaresi *et al.*, Mutants, overexpressors, and interactors of Arabidopsis plastocyanin isoforms: Revised roles of plastocyanin in photosynthetic electron flow and thylakoid redox state. *Mol. Plant* **2**, 236–248 (2009).

24. S. C. Dodani *et al.*, Calcium-dependent copper redistributions in neuronal cells revealed by a fluorescent copper sensor and X-ray fluorescence microscopy. *Proc. Natl. Acad. Sci. U.S.A.* **108**, 5980–5985 (2011).

25. A. Hong-Hermesdorf *et al.*, Subcellular metal imaging identifies dynamic sites of Cu accumulation in Chlamydomonas. *Nat. Chem. Biol.* **10**, 1034–1042 (2014).

26. E. van der Graaff *et al.*, Transcription analysis of *Arabidopsis* membrane transporters and hormone pathways during developmental and induced leaf senescence. *Plant Physiol.* **141**, 776–792 (2006).

27. S. S. Merchant, S. Schmollinger, D. Strenkert, J. L. Moseley, C. E. Blaby-Haas, From economy to luxury: Copper homeostasis in Chlamydomonas and other algae. *Biochim. Biophys. Acta Mol. Cell Res.* **1867**, 118822 (2020).

28. S. Aubry *et al.*, Pheophorbide *a* may regulate Jasmonate signaling during dark-induced senescence. *Plant Physiol.* **182**, 776–791 (2020).

29. J. M. Guss *et al.*, Phase determination by multiple-wavelength x-ray diffraction: Crystal structure of a basic "blue" copper protein from cucumbers. *Science* **241**, 806–811 (1988).

30. A. Jiang *et al.*, The PIF1-miR408-PLANTACYANIN repression cascade regulates light-dependent seed germination. *Plant Cell* **33**, 1506–1529 (2021).

31. A. Van Gysel, M. Van Montagu, D. Inzé, A negatively light-regulated gene from *Arabidopsis thaliana* encodes a protein showing high similarity to blue copper-binding proteins. *Gene* **136**, 79–85 (1993).

32. K. N. Lohman, S. Gan, M. C. John, R. M. Amasino, Molecular analysis of natural leaf senescence in *Arabidopsis thaliana*. *Physiol. Plant.* **92**, 322–328 (1994).

33. L. M. Weaver, S. Gan, B. Quirino, R. M. Amasino, A comparison of the expression patterns of several senescence-associated genes in response to stress and hormone treatment. *Plant Mol. Biol.* **37**, 455–469 (1998).

34. J. Dong, S. T. Kim, E. M. Lord, Plantacyanin plays a role in reproduction in *Arabidopsis*. *Plant Physiol.* **138**, 778–789 (2005).

35. J. Pan *et al.*, Overexpression of microRNA408 enhances photosynthesis, growth, and seed yield in diverse plants. *J. Integr. Plant Biol.* **60**, 323–340 (2018).

36. H. Zhang, L. Li, SQUAMOSA promoter binding protein-like7 regulated microRNA408 is required for vegetative development in *Arabidopsis*. *Plant J.* **74**, 98–109 (2013).

37. H. Zhang *et al.*, MicroRNA408 is critical for the HY5-SPL7 gene network that mediates the coordinated response to light and copper. *Plant Cell* **26**, 4933–4953 (2014).

38. Y. Sakuraba *et al.*, Phytochrome-interacting transcription factors PIF4 and PIF5 induce leaf senescence in *Arabidopsis*. *Nat. Commun.* **5**, 1–13 (2014).

39. Y. Song *et al.*, Age-triggered and dark-induced leaf senescence require the bHLH transcription factors PIF3, 4, and 5. *Mol. Plant* **7**, 1776–1787 (2014).

40. P. Hornitschek *et al.*, Phytochrome interacting factors 4 and 5 control seedling growth in changing light conditions by directly controlling auxin signaling. *Plant J.* **71**, 699–711 (2012).

41. E. Oh, J.-Y. Zhu, Z.-Y. Wang, Interaction between BZR1 and PIF4 integrates brassinosteroid and environmental responses. *Nat. Cell Biol.* **14**, 802–809 (2012).

42. Y. Zhang *et al.*, A quartet of PIF bHLH factors provides a transcriptionally centered signaling hub that regulates seedling morphogenesis through differential expression-patterning of shared target genes in *Arabidopsis*. *PLoS Genet.* **9**, e1003244 (2013).

43. J. Dong *et al.*, *Arabidopsis* DE-ETIOLATED1 represses photomorphogenesis by positively regulating phytochrome-interacting factors in the dark. *Plant Cell* **26**, 3630–3645 (2014).

44. P. Leivar *et al.*, Multiple phytochrome-interacting bHLH transcription factors repress premature seedling photomorphogenesis in darkness. *Curr. Biol.* **18**, 1815–1823 (2008).

45. L. L. Hensel, V. Grbić, D. A. Baumgarten, A. B. Bleecker, Developmental and age-related processes that influence the longevity and senescence of photosynthetic tissues in *Arabidopsis*. *Plant Cell* **5**, 553–564 (1993).

46. R. D. Graham, Male sterility in wheat plants deficient in copper. *Nature* **254**, 514–515 (1975).

47. E. Himelblau, R. M. Amasino, Delivering copper within plant cells. *Curr. Opin. Plant Biol.* **3**, 205–210 (2000).

48. J. Kropat *et al.*, A regulator of nutritional copper signaling in Chlamydomonas is an SBP domain protein that recognizes the GTAC core of copper response element. *Proc. Natl. Acad. Sci. U.S.A.* **102**, 18730–18735 (2005).

49. H. Yamasaki, M. Hayashi, M. Fukazawa, Y. Kobayashi, T. Shikanai, SQUAMOSA promoter binding protein-like7 is a central regulator for copper homeostasis in *Arabidopsis*. *Plant Cell* **21**, 347–361 (2009).

50. Z. Li, J. Peng, X. Wen, H. Guo, Ethylene-insensitive3 is a senescence-associated gene that accelerates age-dependent leaf senescence by directly repressing miR164 transcription in *Arabidopsis*. *Plant Cell* **25**, 3311–3328 (2013).

51. C. Chang, S. F. Kwok, A. B. Bleecker, E. M. Meyerowitz, *Arabidopsis* ethylene-response gene ETR1: Similarity of product to two-component regulators. *Science* **262**, 539–544 (1993).

52. T. Hirayama *et al.*, RESPONSIVE-TO-ANTAGONIST1, a Menkes/Wilson disease-related copper transporter, is required for ethylene signaling in *Arabidopsis*. *Cell* **97**, 383–393 (1999).

53. F. I. Rodríguez *et al.*, A copper cofactor for the ethylene receptor ETR1 from *Arabidopsis*. *Science* **283**, 996–998 (1999).

54. L. Fan, S. Zheng, X. Wang, Antisense suppression of phospholipase D alpha retards abscisic acid- and ethylene-promoted senescence of postharvest *Arabidopsis* leaves. *Plant Cell* **9**, 2183–2196 (1997).

55. H. R. Woo *et al.*, ORE9, an F-box protein that regulates leaf senescence in *Arabidopsis*. *Plant Cell* **13**, 1779–1790 (2001).

56. L. Zeng, E. W. Miller, A. Pralle, E. Y. Isacoff, C. J. Chang, A selective turn-on fluorescent sensor for imaging copper in living cells. *J. Am. Chem. Soc.* **128**, 10–11 (2006).

57. P. Ewels, M. Magnusson, S. Lundin, M. Käller, MultiQC: Summarize analysis results for multiple tools and samples in a single report. *Bioinformatics* **32**, 3047–3048 (2016).

58. M. Pertea, D. Kim, G. M. Pertea, J. T. Leek, S. L. Salzberg, Transcript-level expression analysis of RNA-seq experiments with HISAT, StringTie and Ballgown. *Nat. Protoc.* **11**, 1650–1667 (2016).

59. M. I. Love, W. Huber, S. Anders, Moderated estimation of fold change and dispersion for RNA-seq data with DESeq2. *Genome Biol.* **15**, 550 (2014).

60. B. Langmead, S. L. Salzberg, Fast gapped-read alignment with Bowtie 2. *Nat. Methods* **9**, 357–359 (2012).

61. F. Ramírez *et al.*, deepTools2: A next generation web server for deep-sequencing data analysis. *Nucleic Acids Res.* **44** (W1), W160–W165 (2016).

62. B. Zhang, *Arabidopsis thaliana* seedlings treated with copper sulfate. NCBI BioProject. https://www.ncbi.nlm.nih.gov/bioproject/?term=prjna350795. Accessed 11 January 2019.

Hao et al.
The PCY-SAG14 phytocyanin module regulated by PIFs and miR408
promotes dark-induced leaf senescence in *Arabidopsis*